INTERNATIONAL JOURNAL FOR NUMERICAL METHODS IN ENGINEERING
Int. J. Numer. Meth. Engng 2002; **53**:31–47 (DOI: 10.1002/nme.390)

Singularity treatment and high-order RWG basis functions for integral equations of electromagnetic scattering

W. Cai[1,*,†], Yijun Yu[1] and X. C. Yuan[2]

[1] *Department of Mathematics, University of North Carolina at Charlotte, Charlotte, NC 28223, U.S.A.*
[2] *Rambus Incorporated, 2465 Latham Street, Mountain View, CA 94040, U.S.A.*

SUMMARY

We present numerical implementation of high order RWG basis functions for electromagnetic scattering for curved conductor surfaces with a procedure for treating the singularities of dyadic Green's functions in the mixed potential formulation of electromagnetic scattering. Copyright © 2001 John Wiley & Sons, Ltd.

KEY WORDS: singular integral; RWG basis; high-order basis; electromagnetic scattering; boundary integral method

1. INTRODUCTION

Various numerical techniques have been developed to carry out the electromagnetic field simulation. They include mode matching method based on the eigenmode expansion of the computed object such as a cavity [1], finite difference time-domain (FDTD) using Yee scheme [2], or integral equation formulation [3] with Galerkin-type approximation such as the method of moments (MOM) [4] or point matching method. Among these numerical techniques, the main advantage of the integral formulation is the reduction of solution unknowns and the flexibility in handling very complex geometry of the scatter surface and the automatic enforcement of Sommerfeld exterior decaying conditions [5] by the construction of proper Green's functions. A popular integral equation formulation for electromagnetic fields is the mixed potential (vector and scalar potentials) representation of the fields, such an approach has been found very efficient in handling the singularities from the Green's functions [4, 6].

In this paper, we will present a novel method for treating singularities of the dyadic Green's functions used in the mixed potential formulation of electromagnetic scattering. We will also

*Correspondence to: Wei Cai, Department of Mathematics, University of North Carolina at Charlotte, Charlotte, NC 28223, U.S.A.
†E-mail address: wcai@uncc.edu.

Contract/grant sponsor: NSF; contract/grant numbers: CCR-9972251, CCR-9988375 and CCR0098140

present numerical tests of a newly constructed high-order curved triangular basis function, with the proposed treatment of singularities.

To represent the current vector field over conductor's surfaces, in many cases it is important in a mixed potential integral formulation to have a current vector basis with continuity of the normal components across the interfaces among adjacent elements. The physical justification is that no charge accumulation should occur along the interface between adjacent elements. The triangular Rao–Wilton–Glisson (RWG [6]) basis functions are the most used basis functions with such a property for scattering calculation. In this paper, we continue the study of a newly developed high-order basis [7, 8], which has the following properties (1) it is applicable to either curved or flat triangular and/or quadrilateral patches; (2) it can be higher order while the lowest order, over flat triangular patches, reduces to the usual RWG basis functions; (3) the normal components of the current basis functions are continuous across common interfaces among adjacent patches. High-order basis functions over triangular patches have been attempted in Reference [9], however, no explicit and easy-to-implement formulations of the basis functions of general high-order have been provided. Popovic and Kolundzija studied high-order surface current basis functions in Reference [10] using polynomials of parametric variables of the curved quadrilaterals and triangles with continuous normal component over generalized quadrilaterals and triangles. Later, the approach in Reference [10] was used in Reference [11] to produce high-order of tangential vector finite element (TVFE) basis in the Sobolev space $H(\mathrm{Curl})$ in 2-D and 3-D spaces, similar to the edge elements proposed by Nedelec [12] and studied by others [13, 14].

Method of moments (including Galerkin or collocation methods) using parametric geometry of either triangular or quadrilateral curved patches with RWG basis functions has been used in References [15–17] for electromagnetic (EM) scattering calculations. Vector basis functions in $H(\mathrm{Div})$ was constructed by Raviart and Thomas for solving mixed formulation of Poisson equation [18], and later used in the calculation of eddy current in Reference [19]. The high-order basis functions used in this paper were derived in Reference [8] and hierarchical polynomials of different modes (vertex, edge and interior modes [20]) are used so that the continuities of the normal component of the current basis functions are easily satisfied by choosing appropriate coefficients for the edge mode polynomials.

In addition to using high-order basis functions to achieve better accuracy, it is also important to calculate accurately the singular integrals of the Green's functions. In Reference [21], a subtraction of term like $1/r$ is proposed where an explicit closed form for the integration of $1/r$ over flat triangular or quadrilateral patches is derived. However, the closed form does not apply to curved surfaces. In this paper, we apply the method of local polar co-ordinate transformation to eliminate the singularity effect from terms like $\mathrm{e}^{-\mathrm{j}kr}/r$ completely. Numerical results show the effectiveness of the proposed procedure. The effect of using a polar co-ordinate is similar to that of the so-called Duffy transformation [22, 23] and both methods were analysed in detail in Reference [24].

The rest of the paper is organized as follows. Section 2 presents the formulation of the mixed potential integral equation for the scattering fields of a scatter embedded in a free space. Section 3 provides the construction of the mixed triangular basis functions. Section 4 contains a new treatment for singular integrals, and Section 5 presents some numerical results with high-order basis functions with the proposed treatment of singular integrals. Finally, Section 6 contains the conclusion of the paper.

2. MIXED POTENTIAL INTEGRAL EQUATION (MPIE) AND METHOD OF MOMENTS

Mixed potential integral equation (MPIE) is based on vector and scalar representations of the electric field [25] in terms of the current and charge variables. Integration by parts is used to reduce the singularity of the integral equation. Such a procedure was first tried in Reference [26].

Consider a scatterer V_2 with a surface S of an external normal $\mathbf{n}$, whose complement is denoted by V_1, embedded in an isotropic 3-D space filled with a medium of permittivity ε and permeability μ. For time harmonic fields, where the time dependence is assumed to be $\exp(\mathrm{j}\omega t)$, the dyadic Green's function $\bar{\mathbf{G}}_E(\mathbf{r},\mathbf{r}')$ is

$$\bar{\mathbf{G}}_E(\mathbf{r},\mathbf{r}') = \left[\bar{\mathbf{I}} + \frac{1}{k^2}\nabla\nabla\right] g(R)$$

where $\bar{\mathbf{I}}$ is the identity dyadic and $k^2 = \omega^2\varepsilon\mu$ and

$$g(R) = \frac{\mathrm{e}^{-\mathrm{j}kR}}{4\pi R}, \quad R = |\mathbf{r} - \mathbf{r}'| \tag{1}$$

$\bar{\mathbf{G}}_E(\mathbf{r},\mathbf{r}')$ satisfies the following vector wave equation:

$$\nabla \times \frac{1}{\mu}\nabla \times \bar{\mathbf{G}}_E(\mathbf{r},\mathbf{r}') - \omega^2\varepsilon\bar{\mathbf{G}}_E(\mathbf{r},\mathbf{r}') = \frac{1}{\mu}\bar{\mathbf{I}}\delta(\mathbf{r} - \mathbf{r}'), \quad \mathbf{r} \in V_1 \tag{2}$$

From the Maxwell equations [27], the magnetic dyadic Green's function $\bar{\mathbf{G}}_H(\mathbf{r},\mathbf{r}')$ is

$$\bar{\mathbf{G}}_H(\mathbf{r},\mathbf{r}') = -\frac{1}{\mathrm{j}\omega\mu}\nabla \times \bar{\mathbf{G}}_E(\mathbf{r},\mathbf{r}') \tag{3}$$

namely,

$$\bar{\mathbf{G}}_H(\mathbf{r},\mathbf{r}') = -\frac{1}{\mathrm{j}\omega\mu}\nabla \times \left[\bar{\mathbf{I}} + \frac{1}{k^2}\nabla\nabla\right] g(R) \tag{4}$$

which satisfies

$$\nabla \times \frac{1}{\varepsilon}\nabla \times \bar{\mathbf{G}}_H(\mathbf{r},\mathbf{r}') - \omega^2\mu\bar{\mathbf{G}}_H(\mathbf{r},\mathbf{r}') = \bar{\mathbf{I}}\nabla \times \frac{1}{\mathrm{j}\omega\mu\varepsilon}\delta(\mathbf{r} - \mathbf{r}'), \quad \mathbf{r} \in V_1 \tag{5}$$

Now, from Reference [27], we have the following integral representation for the electromagnetic fields $\mathbf{E}_1, \mathbf{H}_1$ in V_1.

$$\mathbf{E}_1(\mathbf{r}) = \mathbf{E}^{\mathrm{inc}}(\mathbf{r}) - \mu\int_S \mathrm{d}s' \left[\mathrm{j}\omega\mathbf{J}_{\mathrm{e(s)}}(\mathbf{r}') \cdot \bar{\mathbf{G}}_E^1(\mathbf{r}',\mathbf{r}) + \frac{1}{\mu}\mathbf{J}_{\mathrm{m(s)}}(\mathbf{r}') \cdot \nabla \times \bar{\mathbf{G}}_E^1(\mathbf{r}',\mathbf{r})\right], \quad \mathbf{r} \in V_1 \tag{6}$$

where $\bar{\mathbf{G}}_E^1(\mathbf{r}',\mathbf{r})$ is the dyadic Green's functions for the region V_1 and $\mathbf{E}^{\mathrm{inc}}(\mathbf{r})$ is an incident field and the equivalent surface currents over S are defined as

$$\mathbf{J}_{\mathrm{e(s)}}(\mathbf{r}) = \mathbf{n} \times \mathbf{H}_1(\mathbf{r}) \tag{7}$$

$$\mathbf{J}_{\mathrm{m(s)}}(\mathbf{r}) = -\mathbf{n} \times \mathbf{E}_1(\mathbf{r}) \tag{8}$$

with s denoting surface currents.

2.1. MPIE formulations

For a MPIE, the electrical field is expressed in terms of a vector potential $\mathbf{A}$ and a scalar potential V_e, i.e.

$$\mathbf{E} = -j\omega\mathbf{A} - \nabla V_e \tag{9}$$

where

$$\nabla^2\mathbf{A} + k^2\mathbf{A} - \mu\nabla\frac{1}{\mu}\times\nabla\times\mathbf{A} = -\mu\mathbf{J}_e \tag{10}$$

with $\mathbf{J}_e$ being the electric current source. And the Lorentz Gauge condition is used to relate V_e to $\mathbf{A}$, i.e.

$$\nabla\cdot\mathbf{A} = -j\omega\varepsilon\mu V_e \tag{11}$$

Thus, V_e satisfies the following Helmholtz equation

$$\nabla^2 V_e + k^2 V_e = -\frac{1}{\varepsilon}\rho_e \tag{12}$$

where the electric charge ρ_e is related to $\mathbf{J}_e$ by the continuity equation,

$$\rho_e = -\frac{1}{j\omega}\nabla\cdot\mathbf{J}_e \tag{13}$$

It is easy to show that the dyadic Green's function for the vector is

$$\bar{\mathbf{G}}_A(\mathbf{r},\mathbf{r}') = -\frac{1}{j\omega}g(R)\bar{\mathbf{I}} \tag{14}$$

From Equation (6), the electric field $\mathbf{E}_1$ in V_1 can be expressed in terms of both the tangential components of electric and magnetic fields (namely, equivalent currents $\mathbf{J}_{m(s)}$ and $\mathbf{J}_{e(s)}$) over the scatter surface S. According to the impedance boundary condition for conductors [28], we have a relation between these two currents,

$$\mathbf{J}_{m(s)} = -Z_s\mathbf{n}\times\mathbf{J}_{e(s)} \tag{15}$$

Now for a perfect electric conductor (PEC) $Z_s = 0$, we have $\mathbf{J}_{m(s)} = 0$ and

$$\mathbf{n}\times\mathbf{E}_1 = \mathbf{n}\times(\mathbf{E}^s + \mathbf{E}^{inc}) = 0 \tag{16}$$

where $\mathbf{E}^s$ is the scattered field. Finally, we have the following MPIE:

$$\mathbf{n}\times j\omega\mu\left[j\omega\int_S\bar{\mathbf{G}}_A\cdot\mathbf{J}_s\,ds' - \nabla\cdot\int_S\frac{j\omega}{k^2}\nabla\bar{\mathbf{G}}_A\cdot\mathbf{J}_s\,ds'\right] = -\mathbf{n}\times\mathbf{E}^{inc}, \quad \mathbf{r}\in V_1 \tag{17}$$

where $\mathbf{J}_s = \mathbf{J}_{e(s)}$.

Applying integration by parts for the second term in (17), and using the continuity of the normal component of the surface current $\mathbf{J}_s$ and the continuity equation (13) for the surface electric current $\mathbf{J}_s$ and surface charge ρ_s, we have

$$\mathbf{n}\times j\omega\mu\left[-\int_S g(R)\mathbf{J}_s(\mathbf{r}')\,ds' + \frac{j\omega}{k^2}\nabla\cdot\int_S g(R)\rho_s(\mathbf{r}')\,ds'\right] = -\mathbf{n}\times\mathbf{E}^{inc}, \quad \mathbf{r}\in V_1 \tag{18}$$

Such a formulation reduces the degree of the singularities of the surface integration, and a Galerkin procedure will be applied to (18) where the current $\mathbf{J}_s$ and charge ρ_s are expressed in terms of N terms of high-order RWG basis function, namely

$$\mathbf{J}_s(\mathbf{r}) = \sum_{k=1}^{N} I_k \mathbf{J}_k(\mathbf{r})$$

and

$$\rho_s(\mathbf{r}) = \sum_{k=1}^{N} I_k \rho_k(\mathbf{r})$$

where $\rho_k(\mathbf{r}) = -(1/\mathrm{j}\omega)\nabla \cdot \mathbf{J}_k(\mathbf{r})$.

A Galerkin projection procedure will yield the following algebraic equation

$$\sum_{l=1}^{N} Z_{kl} I_l = V_k, \quad k = 1, 2, 3, \ldots, N \tag{19}$$

where, after using integration by part to transfer the gradient operator ∇ in (18) to the test function $\mathbf{J}_l(\mathbf{r}')$, and using the continuity equation (13), we have

$$Z_{kl} = \mathrm{j}\omega\mu \left[\int_S \int_S g(R) \mathbf{J}_k(\mathbf{r}) \cdot \mathbf{J}_l(\mathbf{r}') \, \mathrm{d}s \, \mathrm{d}s' + \frac{1}{\varepsilon\mu} \int_S \int_S g(R) \rho_k(\mathbf{r}) \rho_l(\mathbf{r}') \, \mathrm{d}s \, \mathrm{d}s' \right] \tag{20}$$

and

$$V_k = \int_S \mathbf{E}^{\mathrm{inc}} \cdot \mathbf{J}_k(\mathbf{r}) \, \mathrm{d}s \tag{21}$$

3. HIGH-ORDER RWG BASIS FUNCTIONS

In arriving at (20), Equation (17) is multiplied by a test function $\mathbf{J}_l(\mathbf{r})$ and then, integrated over the surface S. In order to transfer the ∇ operator in the second term in (18) to the test function via integration by parts, normal continuity of $\mathbf{J}_l(\mathbf{r})$ is needed across the common interface of triangular patches. In this section, we will present such a current basis function, the normal continuity of the current basis function is the key property of the popular RWG basis functions, which ensures no accumulation of charges across the element interfaces. In the following, we will give the formulation of higher order extension of the original RWG basis over arbitrary triangular curved patches. The details of the derivation of the basis function can be found in References [7, 8]

Let Σ be a curved triangular surface in $\mathbb{R}^3$ and Σ is parameterized by $\mathbf{x} = \mathbf{x}(u_1, u_2), (u_1, u_2) \in T_0$, T_0 is a standard reference triangle in Figure 1.

Tangential vectors: $\partial_i \mathbf{x}$, $i = 1, 2$ are defined as

$$\partial_i \mathbf{x} = \frac{\partial \mathbf{x}}{\partial u_i}, \quad i = 1, 2 \tag{22}$$

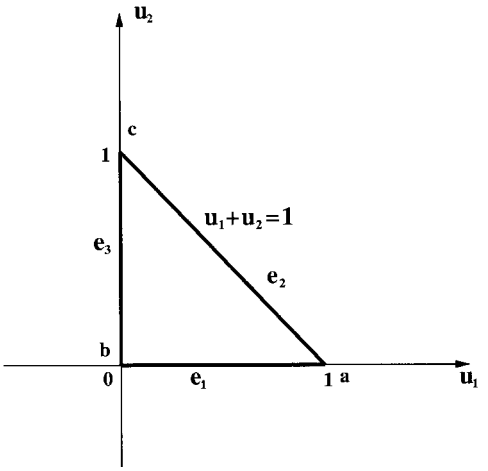

Figure 1. Reference triangle T_0.

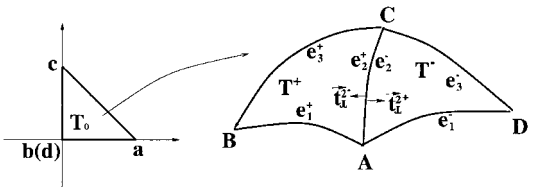

Figure 2. Left: reference triangle T_0, Right: curved triangular and triangular patches.

Metric tensor: The distance between two points on Σ parameterized by (u_1, u_2) and $(u_1 + \mathrm{d}u_1, u_2 + \mathrm{d}u_2)$ is given by

$$(\mathrm{d}s)^2 = g_{\mu\nu}(u)\,\mathrm{d}u_\mu\,\mathrm{d}u_\nu \tag{23}$$

where repeated indices imply summation

$$g_{\mu\nu} = \frac{\partial \mathbf{x}}{\partial u_\mu} \cdot \frac{\partial \mathbf{x}}{\partial u_\nu}, \quad 1 \leqslant \mu, \quad \nu \leqslant 2 \tag{24}$$

and $\{g_{\mu\nu}\}$ is defined as the covariant tensor [29]. The determinant of $\{g_{\mu\nu}\}$ is denoted by

$$g = \det\{g_{\mu\nu}\} = g_{11}g_{22} - g_{12}^2 = \|\partial_1 \mathbf{x} \times \partial_2 \mathbf{x}\|^2 \tag{25}$$

3.1. Hierarchical polynomial basis over triangle T_0

Let T_0 be the reference triangle with vertices a, b, c in Figure 1, we group (u_1, u_2) polynomials into three modes: vertex modes, edge modes and internal modes [20].

Vertex mode:

$$\begin{aligned} g_a(u_1, u_2) &= u_1 \\ g_b(u_1, u_2) &= 1 - u_1 - u_2 \\ g_c(u_1, u_2) &= u_2 \end{aligned} \tag{26}$$

Each vertex mode will take value 1 at one vertex and zero at other two vertices.

Edge modes: for $2 \leqslant l \leqslant M$

$$\begin{aligned} g_l^{ab}(u_1,u_2) &= g_a(u_1,u_2)g_b\ (u_1,u_2)p_{l-2}(g_b-g_a) \\ g_l^{bc}(u_1,u_2) &= g_b(u_1,u_2)g_c(u_1,u_2)p_{l-2}(g_c-g_b) \\ g_l^{ca}(u_1,u_2) &= g_c(u_1,u_2)g_a(u_1,u_2)p_{l-2}(g_a-g_c) \end{aligned} \tag{27}$$

where $p_l(\xi), \xi \in [-1,1]$ is lth order Legendre polynomial.
Each of the edge mode is only non-zero along one edge of the triangle T_0.

Internal modes: $0 \leqslant k+l \leqslant M-3$

$$g_{l,k}^{\text{int}}(u_1,u_2) = g_a(u_1,u_2)g_b(u_1,u_2)g_c(u_1,u_2)p_k(2g_c-1)p_l(g_b-g_a)$$

and each of the internal mode will vanish over all edges of T_0.

3.2. High-order current basis functions over curved triangular patches

Consider two curved triangular patches T^+ and T^- with a common interface AC with length ℓ in Figure 2. Let T^+ and T^- be parameterized, respectively, by

$$\mathbf{x} = \mathbf{x}^+(u_1,u_2) : T_0 \to T^+ \tag{29}$$

$$\mathbf{x} = \mathbf{x}^-(u_1,u_2) : T_0 \to T^- \tag{30}$$

We assume that the interface AC in both T^+ and T^- is parameterized by $u_1+u_2=1$ and is labelled as side e_2^+ in T^+ and side e_2^- in T^-.

In Reference [8], the following basis functions with continuous normal components are constructed.

RWG basis. If we assume that the normal component of the current basis function remains constant along the interface AC in the case of plane triangles, we have

$$\mathbf{f}(\mathbf{x}) = I_n \begin{cases} \dfrac{l}{\sqrt{g^+}}(g_A(u_1,u_2)\partial_1\mathbf{x} + g_C(u_1,u_2)\partial_2\mathbf{x}) & \text{if } \mathbf{x}=\mathbf{x}^+(u_1,u_2) \in T^+ \\ \dfrac{l}{\sqrt{g^-}}(-g_A(u_1,u_2)\partial_1\mathbf{x} - g_C(u_1,u_2)\partial_2\mathbf{x}) & \text{if } \mathbf{x}=\mathbf{x}^-(u_1,u_2) \in T^- \end{cases} \tag{31}$$

and for flat triangle patches, we have in T^+

$$\mathbf{x} = \mathbf{x}^+(u_1,u_2) = g_A(u_1,u_2)\mathbf{x}_A + g_B(u_1,u_2)\mathbf{x}_B + g_C(u_1,u_2)\mathbf{x}_C \tag{32}$$

$$\begin{aligned} \partial_1\mathbf{x} &= \mathbf{x}_A - \mathbf{x}_B \\ \partial_2\mathbf{x} &= \mathbf{x}_C - \mathbf{x}_B \end{aligned} \tag{33}$$

and in T^-

$$\mathbf{x} = \mathbf{x}^-(u_1,u_2) = g_A(u_1,u_2)\mathbf{x}_A + g_D(u_1,u_2)\mathbf{x}_D + g_C(u_1,u_2)\mathbf{x}_C \tag{34}$$

where $g_D(u_1,u_2)=g_B(u_1,u_2)$,

$$\begin{aligned}\partial_1\mathbf{x}&=\mathbf{x}_A-\mathbf{x}_D\\ \partial_2\mathbf{x}&=\mathbf{x}_C-\mathbf{x}_D\end{aligned}\tag{35}$$

Thus, we have the RWG basis function

$$\mathbf{f}(\mathbf{x})=I_n\begin{cases}\dfrac{l}{2A^+}(\mathbf{x}-\mathbf{x}_B) & \text{if } \mathbf{x}=\mathbf{x}^+(u_1,u_2)\in T^+\\ -\dfrac{l}{2A^-}(\mathbf{x}-\mathbf{x}_D) & \text{if } \mathbf{x}=\mathbf{x}^-(u_1,u_2)\in T^-\end{cases}\tag{36}$$

where A^+ and A^- are the areas of triangles $T^+$and T^-, respectively.

The unknown for each edge AC is just I_n.

First-order basis. In this case, we allow the normal component of the current basis function to vary along the edge

$$\mathbf{f}(\mathbf{x})=\begin{cases}\dfrac{l}{\sqrt{g^+}}(I_n^a g_A(u_1,u_2)\partial_1\mathbf{x}+I_n^c g_C(u_1,u_2)\partial_2\mathbf{x}) & \text{if } \mathbf{x}=\mathbf{x}^+(u_1,u_2)\in T^+\\ \dfrac{l}{\sqrt{g^-}}(-I_n^a g_A(u_1,u_2)\partial_1\mathbf{x}-I_n^c g_C(u_1,u_2)\partial_2\mathbf{x}) & \text{if } \mathbf{x}=\mathbf{x}^-(u_1,u_2)\in T^-\end{cases}\tag{37}$$

The unknowns for each edge AC are I_n^a, I_n^c.

Second-order basis:

$$\mathbf{f}(\mathbf{x})=\begin{cases}\dfrac{l}{\sqrt{g^+}}\left\{\left[I_n^a g_A(u_1,u_2)+\dfrac{I_n^{(2)}-\tilde{I}_t^{(2)}}{2}g_2^{e_2^+}(u_1,u_2)\right]\partial_1\mathbf{x}\right.\\ \qquad\left.+\left[I_n^c g_C(u_1,u_2)+\dfrac{I_n^{(2)}+\tilde{I}_t^{(2)}}{2}g_2^{e_2^+}(u_1,u_2)\right]\partial_2\mathbf{x}\right\} & \text{if } \mathbf{x}=\mathbf{x}^+(u_1,u_2)\in T^+\\ \dfrac{l}{\sqrt{g^-}}\left\{\left[-I_n^a g_A(u_1,u_2)+\dfrac{-I_n^{(2)}-\hat{I}_t^{(2)}}{2}g_2^{e_2^-}(u_1,u_2)\right]\partial_1\mathbf{x}\right.\\ \qquad\left.+\left[-I_n^c g_C(u_1,u_2)+\dfrac{-I_n^{(2)}+\hat{I}_t^{(2)}}{2}g_2^{e_2^-}(u_1,u_2)\right]\partial_2\mathbf{x}\right\} & \text{if } \mathbf{x}=\mathbf{x}^-(u_1,u_2)\in T^-\end{cases}\tag{38}$$

where $e_2^-=e_2^+=ca$. The unknowns for each edge AC are $I_n^a, I_n^c, I_n^{(2)}, \hat{I}_t^{(2)}, \tilde{I}_t^{(2)}$.

Higher order current basis function can be found in the appendix and the details of construction in References [7, 8].

4. TREATMENT OF SINGULAR INTEGRALS

If the scattering surface S is partitioned into N disjoint curved triangular patches $T_j \in \mathscr{T}_h$, i.e. $S = \bigcup_{T_j \in \mathscr{T}_h} T_j$, then from (20), we can see that the matrix element Z_{kl} involves the calculation of integral of the following type,

$$I_{i,j} = \int_{T_i} \int_{T_j} \frac{f(\mathbf{x}) g(\mathbf{x}')}{|\mathbf{x} - \mathbf{x}'|} \mathrm{e}^{-\mathrm{j}k|\mathbf{x}-\mathbf{x}'|} \, \mathrm{d}\mathbf{x} \, \mathrm{d}\mathbf{x}' \tag{39}$$

where $f(\mathbf{x}), g(\mathbf{x})$ will be functions depending on the basis functions. $I_{i,j}$ will be singular when $T_i = T_j$ or behaves badly when T_i is close to T_j. It is important that we evaluate integral $I_{i,j}$ as accurately as possible to achieve the full accuracy of high-order methods.

Let T_0 be a standard reference triangle on (u_1, u_2) plane, see Figure 1. For $T_i \in \mathscr{T}_h$, we define

$$S_i = \{T_j \mid T_j \in \mathscr{T}_h, \mathrm{dist}(T_i, T_j) = 0\} \tag{40}$$

Now consider integral (39) I_{ij}, where $T_j \in S_i$.

For any $T_i \in \mathscr{T}_h$, let there exist one-to-one transformation $\mathbf{x}_{is}(u_1, u_2)$ which maps $U_i \supset T_0$ on (u_1, u_2) plane onto $\Omega_i \supset \bigcup_{T_j \in S_i} T_j$ on S and satisfies

$$\mathbf{x}_{is} : (u_1, u_2) \in T_0 \xrightarrow{onto} \mathbf{x}_{is}(u_1, u_2) \in T_i$$

Let

$$g_i(u_1, u_2) = (\partial_1 \mathbf{x}_{is} \cdot \partial_1 \mathbf{x}_{is})(\partial_2 \mathbf{x}_{is} \cdot \partial_2 \mathbf{x}_{is}) - (\partial_1 \mathbf{x}_{is} \cdot \partial_2 \mathbf{x}_{is})^2 \tag{41}$$

and

$$g_j(u_1, u_2) = (\partial_1 \mathbf{x}_{js} \cdot \partial_1 \mathbf{x}_{js})(\partial_2 \mathbf{x}_{js} \cdot \partial_2 \mathbf{x}_{js}) - (\partial_1 \mathbf{x}_{js} \cdot \partial_2 \mathbf{x}_{js})^2 \tag{42}$$

then

$$\begin{aligned} I_{ij} &= \int_{T_i} \left(\int_{T_j} \frac{f(\mathbf{x}) g(\mathbf{x}')}{|\mathbf{x} - \mathbf{x}'|} \mathrm{e}^{-\mathrm{j}k|\mathbf{x}-\mathbf{x}'|} \, \mathrm{d}\mathbf{x}' \right) \mathrm{d}\mathbf{x} \\ &= \int_{T_0} \int_{T_0} \frac{f(\mathbf{x}_{is}(u_1, u_2)) g(\mathbf{x}_{js}(u_1', u_2'))}{|\mathbf{x}_{is}(u_1, u_2) - \mathbf{x}_{js}(u_1', u_2')|} \\ &\quad \times \mathrm{e}^{-\mathrm{j}k|\mathbf{x}_{is}(u_1,u_2) - \mathbf{x}_{js}(u_1',u_2')|} \sqrt{g_j(u_1', u_2')} \, \mathrm{d}\mathbf{u}' \sqrt{g_i(u_1, u_2)} \, \mathrm{d}\mathbf{u} \\ &= \int_{T_0} \tilde{I}_{ij}(u_1, u_2) \sqrt{g_i(u_1, u_2)} \, \mathrm{d}\mathbf{u} \end{aligned} \tag{43}$$

where

$$\tilde{I}_{ij}(u_1,u_2)=\int_{T_0}\frac{f(\mathbf{x}_{is}(u_1,u_2))g(\mathbf{x}_{js}(u_1',u_2'))}{|\mathbf{x}_{is}(u_1,u_2)-\mathbf{x}_{js}(u_1',u_2')|}\times \mathrm{e}^{-\mathrm{j}k|\mathbf{x}_{is}(u_1,u_2)-\mathbf{x}_{js}(u_1',u_2')|}\sqrt{g_j(u_1',u_2')}\,\mathrm{d}\mathbf{u}' \tag{44}$$

The integration over T_0 in (43) can be evaluated by a Gauss quadrature over triangles [30]. However, the integrand of $\tilde{I}_{ij}(u_1,u_2)$ in (44) itself involves integrating a singular function when $T_i=T_j$. In addition, when $T_i\neq T_j$ with $\mathrm{dist}(T_i,T_j)=0$, the integrand of $\tilde{I}_{ij}$ is not singular, but the result of numerical integral is generally bad. In the following, we will transform the integration $\tilde{I}_{ij}$ into a local polar co-ordinate system (ρ,θ) in the (u_1,u_2) plane such that the singularity of the integrand will be cancelled by the Jacobian of the transformation.

Let

$$\begin{aligned}&F(u_1,u_2,u_1^0,u_2^0,\rho,\theta)\\&\quad=f(\mathbf{x}_{is}(u_1,u_2))g(\mathbf{x}_{js}(\rho\cos\theta+u_1^0,\rho\sin\theta+u_2^0))\\&\qquad\times\mathrm{e}^{-\mathrm{j}k|\mathbf{x}_{is}(u_1,u_2)-\mathbf{x}_{js}(\rho\cos\theta+u_1^0,\rho\sin\theta+u_2^0)|}\sqrt{g_j(\rho\cos\theta+u_1^0,\rho\sin\theta+u_2^0)}\\&\qquad\times\frac{\rho}{|\mathbf{x}_{is}(u_1,u_2)-\mathbf{x}_{js}(\rho\cos\theta+u_1^0,\rho\sin\theta+u_2^0)|}\end{aligned} \tag{45}$$

Now we convert the integration in (u_1',u_2') of $\tilde{I}_{ij}(u_1,u_2)$ to a polar co-ordinate (ρ,θ) centred at (u_1^0,u_2^0), then we have the following conclusions:

(1) For the case $T_i=T_j$, let $(u_1^0,u_2^0)=\mathbf{x}_{js}^{-1}(\mathbf{x}_{is}(u_1,u_2))=(u_1,u_2)$, then

$$\begin{aligned}\tilde{I}_{ij}(u_1,u_2)=&\int_{-\pi+\mathrm{arctg}\,(u_2^0/u_1^0)}^{-\mathrm{arctg}\,(u_2^0/(1-u_1^0))}\int_0^{-u_2^0/\sin\theta}F(u_1,u_2,u_1^0,u_2^0,\rho,\theta)\,\mathrm{d}\rho\,\mathrm{d}\theta\\&+\int_{-\mathrm{arctg}\,(u_2^0/1-u_1^0)}^{\pi-\mathrm{arctg}\,((1-u_2^0)/u_1^0)}\int_0^{(1-u_1^0-u_2^0)/(\sin\theta+\cos\theta)}F(u_1,u_2,u_1^0,u_2^0,\rho,\theta)\,\mathrm{d}\rho\,\mathrm{d}\theta\\&+\int_{\pi-\mathrm{arctg}\,((1-u_2^0)/u_1^0)}^{\pi+\mathrm{arctg}\,(u_2^0/u_1^0)}\int_0^{-u_1^0/\cos\theta}F(u_1,u_2,u_1^0,u_2^0,\rho,\theta)\,\mathrm{d}\rho\,\mathrm{d}\theta\end{aligned} \tag{46}$$

(2) For the case $T_i\neq T_j$ with $\mathrm{dist}(T_i,T_j)=0$, let $(\bar{u}_1,\bar{u}_2)=\mathbf{x}_{js}^{-1}(\mathbf{x}_{is}(u_1,u_2))$ and (u_1^0,u_2^0) is chosen as the closest point on boundary of T_0 to $(\bar{u}_1,\bar{u}_2)$, then we have

(i) $(u_1^0,u_2^0)=(0,1)$

$$\tilde{I}_{ij}(u_1,u_2)=\int_{\pi/2}^{-\pi/4}\int_0^{-1/\sin\theta}F(u_1,u_2,u_1^0,u_2^0,\rho,\theta)\,\mathrm{d}\rho\,\mathrm{d}\theta \tag{47}$$

(ii) $(u_1^0, u_2^0) = (0,0)$

$$\tilde{I}_{ij}(u_1,u_2) = \int_0^{\pi/2} \int_0^{-1/(\sin\theta+\cos\theta)} F(u_1,u_2,u_1^0,u_2^0,\rho,\theta)\,\mathrm{d}\rho\,\mathrm{d}\theta \tag{48}$$

(iii) $(u_1^0, u_2^0) = (1,0)$

$$\tilde{I}_{ij}(u_1,u_2) = \int_{3\pi/4}^{\pi} \int_0^{-1/\cos\theta} F(u_1,u_2,u_1^0,u_2^0,\rho,\theta)\,\mathrm{d}\rho\,\mathrm{d}\theta \tag{49}$$

(iv) (u_1^0, u_2^0) is between point $(0,1)$ and point $(0,0)$, i.e. $(u_1^0, u_2^0) = (0, \bar{u}_2)$

$$\begin{aligned}\tilde{I}_{ij}(u_1,u_2) = &\int_{-\pi/2}^{-\operatorname{arctg} u_2^0} \int_0^{-u_2^0/\sin\theta} F(u_1,u_2,u_1^0,u_2^0,\rho,\theta)\,\mathrm{d}\rho\,\mathrm{d}\theta \\ &+ \int_{-\operatorname{arctg} u_2^0}^{\pi/2} \int_0^{(1-u_2^0)/(\sin\theta+\cos\theta)} F(u_1,u_2,u_1^0,u_2^0,\rho,\theta)\,\mathrm{d}\rho\,\mathrm{d}\theta\end{aligned} \tag{50}$$

(v) (u_1^0, u_2^0) is between point $(0,0)$ and point $(1,0)$, i.e. $(u_1^0, u_2^0) = (\bar{u}_1, 0)$

$$\begin{aligned}\tilde{I}_{ij}(u_1,u_2) = &\int_0^{\pi-\operatorname{arctg}(1/u_1^0)} \int_0^{(1-u_1^0)/(\sin\theta+\cos\theta)} F(u_1,u_2,u_1^0,u_2^0,\rho,\theta)\,\mathrm{d}\rho\,\mathrm{d}\theta \\ &+ \int_{\pi-\operatorname{arctg}(1/u_1^0)}^{\pi} \int_0^{u_1^0/\cos\theta} F(u_1,u_2,u_1^0,u_2^0,\rho,\theta)\,\mathrm{d}\rho\,\mathrm{d}\theta\end{aligned} \tag{51}$$

(vi) (u_1^0, u_2^0) is between point $(0,1)$ and point $(1,0)$, i.e. $u_1^0 = (\bar{u}_1 - \bar{u}_2 + 1)/2$, $u_2^0 = (\bar{u}_2 - \bar{u}_1 + 1)/2$

$$\begin{aligned}\tilde{I}_{ij}(u_1,u_2) = &\int_{3\pi/4}^{\pi+\operatorname{arctg}(u_2^0/u_1^0)} \int_0^{-u_1^0/\cos\theta} F(u_1,u_2,u_1^0,u_2^0,\rho,\theta)\,\mathrm{d}\rho\,\mathrm{d}\theta \\ &+ \int_{\pi+\operatorname{arctg}(u_2^0/u_1^0)}^{7\pi/4} \int_0^{-u_2^0/\sin\theta} F(u_1,u_2,u_1^0,u_2^0,\rho,\theta)\,\mathrm{d}\rho\,\mathrm{d}\theta\end{aligned} \tag{52}$$

It can be shown that $F(u_1,u_2,u_1^0,u_2^0,\rho,\theta)$ is a smooth function of arguments ρ and θ for fixed u_1, u_2, u_1^0 and u_2^0 if only $\mathbf{x}_{js}(u_1,u_2)$ satisfies that $|\mathbf{x}_{js}(u_1,u_2) - \mathbf{x}_{js}(v_1,v_2)| = O(|(u_1,u_2)-(v_1,v_2)|)$, thus $\tilde{I}_{ij}(u_1,u_2)$ can be accurately evaluated by one dimensional Gauss quadratures.

5. NUMERICAL RESULTS—SCATTERING OF A SPHERE

In this section, we will present numerical results of the scattering of a sphere of an incident wave $\mathbf{E}^{\mathrm{inc}}$ using the high-order basis functions and the treatment of singular integral discussed in Sections 4 and 5. We will compute the scattering of a 3-D perfect conducting sphere, for

which a Mie series solution is available for comparison [1]. Numerical results are presented to address various issues of implementing the high-order basis function and the treatment of singular integrals.

A sphere with perfect conducting surface ($Z_s = 0$) is impacted by an incident wave $\mathbf{E}^{\text{inc}}$, and a surface current $\mathbf{J}_s$ will be induced over the surface S of the sphere. We assume that the incident wave is plane wave, i.e.

$$\mathbf{E}^{\text{inc}}(\mathbf{r}) = E_0 \mathbf{u}_x e^{-j\mathbf{k}\cdot\mathbf{r}}$$

where $\mathbf{u}_x$ is the unit vector of x-co-ordinate and $E_0 = 1.5$ and the propagation vector $\mathbf{k}$ is

$$\mathbf{k} = k(\sin\theta_0 \cos\varphi_0, \sin\theta_0 \sin\varphi_0, \cos\theta_0)$$

with $\theta_0 = 0$. In our numerical test the radius of the sphere $a = (1/\pi)\lambda$, where wavelength $\lambda = 2\pi/k$, $k = \omega\sqrt{\varepsilon\mu}$, frequency $f = 135$ MHz, the dielectric constant and permeability of medium are $\varepsilon = 2\varepsilon_0, \mu = \mu_0$ with ε_0, μ_0 being the dielectric constant and permeability of the vacuum, respectively.

The various computation parameters are:

M: order of the numerical methods, $M = 0$ denotes the original RWG basis
N: the number of edges of all triangle patches of the sphere

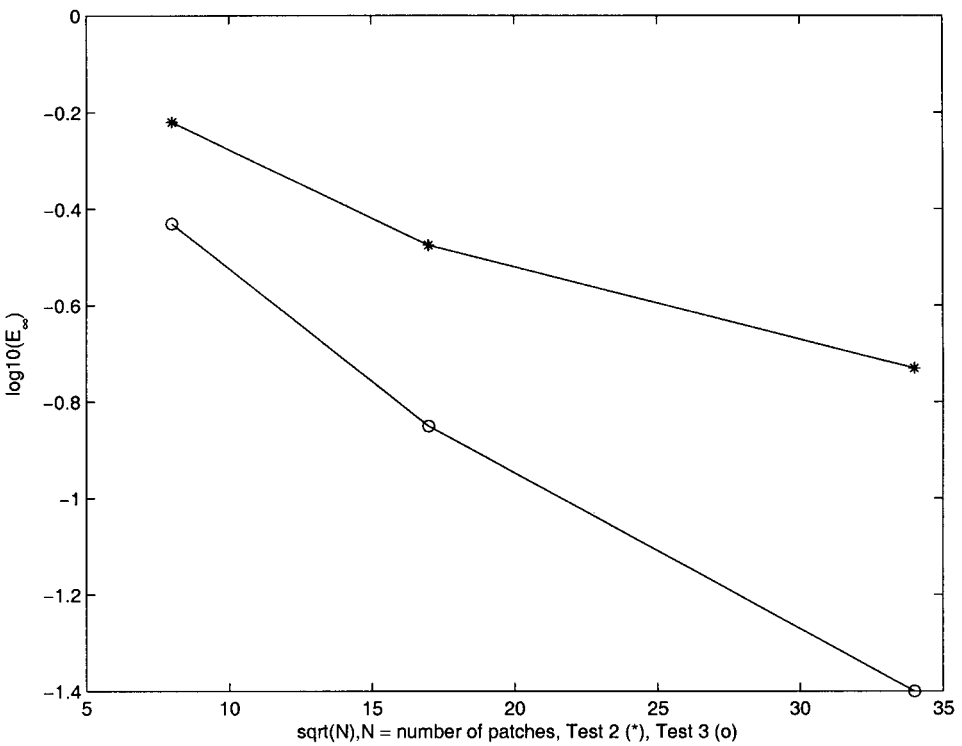

Figure 3. Convergence of RWG basis (top) and first-order basis (bottom) ($N = 72, 288, 1152$).

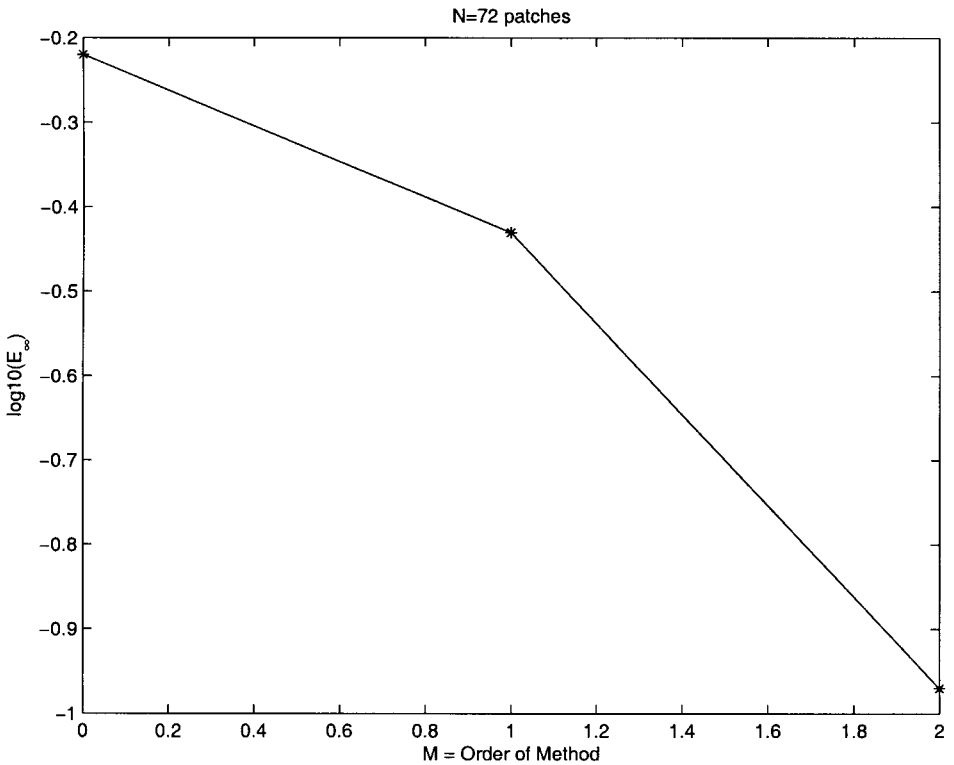

Figure 4. Comparison of RWG, first-order and second-order methods ($N = 72$).

q_{2d}: $q_{2d} = 10$, degree of Gauss quadrature over triangle [30] for the evaluation of (43)
q_{1d}: $q_{1d} = 5$, number of Gauss quadrature points over $[-1, 1]$ for the evaluation of (46)–(52)
E_∞: Maximum error for the surface currents, i.e

$$E_\infty = \max \mid \mathbf{J}_{\mathrm{s,app}} - \mathbf{J}_{\mathrm{s,ex}} \mid$$

where the maximum is taken over all triangle patches and $\mathbf{J}_{\mathrm{s,app}}$ is the numerical solution and $\mathbf{J}_{\mathrm{s,ex}}$ is the solution obtained by the Mie series [1].

Test One: *Comparison between flat and curved triangles* ($M = 2, N = 72$). The error in integral equation methods comes from two sources: One from the discretization of the scatter surfaces, the second from the approximation of the solution space. In this test, we will compare the numerical results of second-order method with flat triangles and curved triangles. In the case of curved triangles, exact sphere surface geometry is used in the definition of the basis function; therefore, no error is committed from the discretization of the surface.

The maximum error for the former is $\log_{10}(E_\infty) = -0.354$ while for the latter $\log_{10}(E_\infty) = -0.975$.

Test Two: *Convergence of RWG basis* ($M = 0, N = 72, 288, 1152$). The RWG basis assumes that the normal component of the current is constant across the element interfaces; therefore,

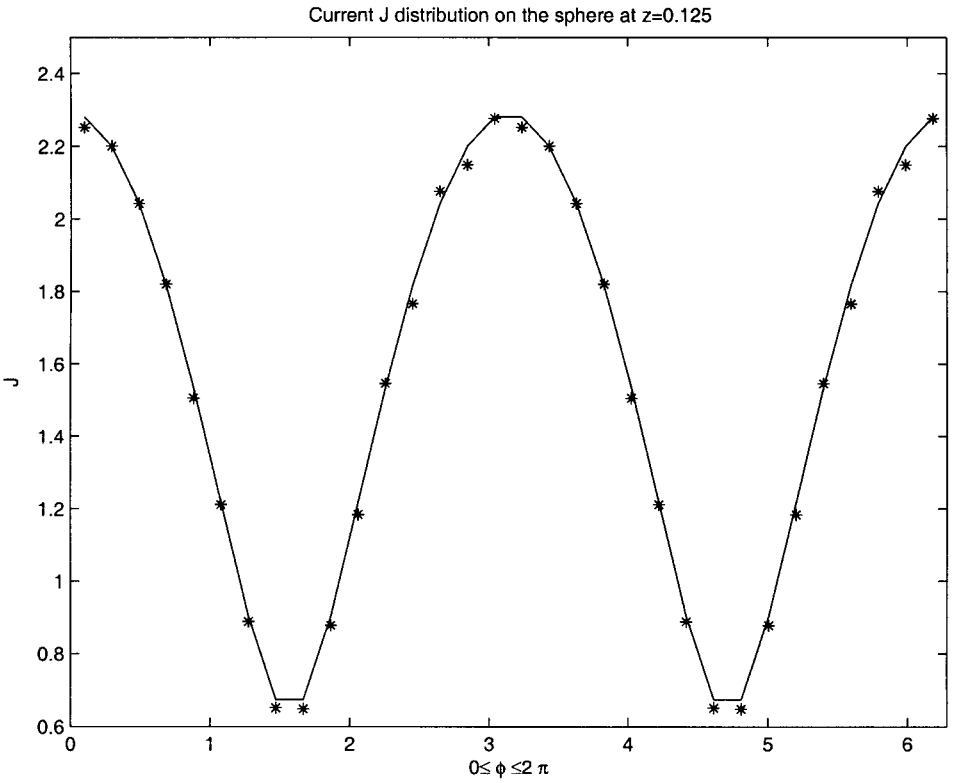

Figure 5. Current distribution over the sphere at $z = 0.125$, (*) computed solution, (-) exact solution.

the basis function cannot reproduce complete first-order polynomial representation for the current solutions. Meanwhile, the convergence rate for the Mth order basis function proposed in this paper should be $O(h^{M+1}), h$ being the average size of the triangle patches.

Figure 3 shows the pointwise error of RWG basis for three different triangulations of the sphere with curved triangles, the maximum errors $\log_{10}(E_\infty)$ for $N = 72, 288, 1152$ are $-0.236, -0.475$ and -0.725, respectively, which indicates a convergence rate of approximately $O(h^{0.8})$.

Test Three: *Convergence of First Order Basis* ($M = 1, N = 72, 288, 1152$). Figure 3 shows the pointwise error of first basis for three different triangulations of the sphere with curved triangles, the maximum errors $\log_{10}(E_\infty)$ for $N = 72, 288, 1152$ are -0.430, -0.847 and -1.405, respectively, which indicates a convergence rate of approximately $O(h^{1.8})$.

Test Four: *Comparison of Different Order Bases* ($M = 0, 1, 2$). In this test, we compare the accuracy of RWG basis ($M = 0$), first-order method ($M = 1$) and second-order method ($M = 2$) with $N = 72$, their maximum error $\log_{10}(E_\infty)$ in the surface currents are $-0.236, -0.430$ and -0.975, respectively (see Figure 4). There is much improvement of the maximum error as the order of the method is increased.

In Figure 5, we plot the current distribution over the sphere at $z = 0.125$, the horizontal axis is ϕ in the spherical co-ordinate (ρ, θ, ϕ) for the points on the sphere, the computed

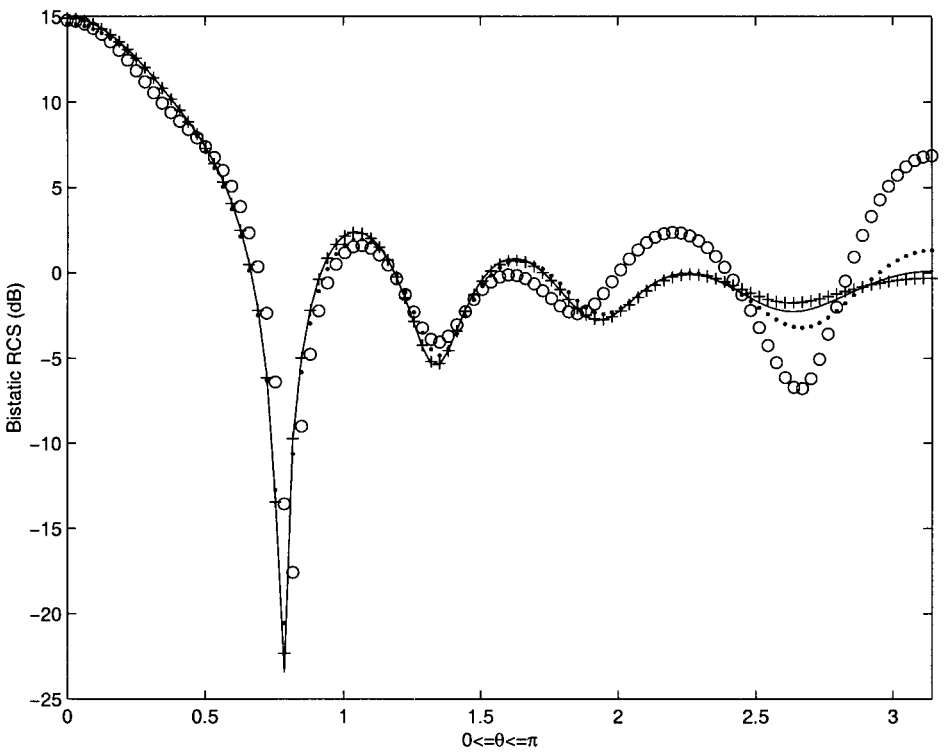

Figure 6. Bistatic RCS by RWG (o), first-order (.) and second order (+) methods ($N = 288$); Solid line—exact solution.

solutions (*) by the second-order method $M = 2$ with $N = 288$ agree well with the exact solution (line).

Finally, in Figure 6, we show the bistatic RCS for the three methods with $N = 288$. The radius of the sphere $a = (3/\pi)\lambda$, where wavelength $\lambda = 2\pi/k$, $k = \omega\sqrt{\varepsilon\mu}$, frequency $f = 572.6$ MHz, the dielectric constant and permeability of medium are $\varepsilon = \varepsilon_0$, $\mu = \mu_0$. The solid line is the exact solution by Mie series, where the circles ($\circ$) are the solution by the original RWG basis, the dots ($\cdot$) are by the first-order method, and the plus (+) are by the second-order methods. It clearly shows the advantage of higher order methods.

6. CONCLUSION

We have demonstrated the accuracy and efficiency of high-order RWG basis functions and the effectiveness of the singularity treatment for mixed potential integral equation methods for electromagnetic scattering.

For basis function of order $M < 3$, the size of the method of moment matrix from the integral equation method is about NL (N is the number of edges, L is the number of basis functions per edge). For $M \geqslant 3$, the matrix size will be larger as we will have additional basis

function which is associated with the interior of the triangles. Based on the numerical tests presented here, for $M<3$, it is more efficient to increase the degree of the basis function for better accuracy than increasing the number of triangles, as shown in Test 4. However, it has also been observed that to maintain the higher order accuracy, appropriate higher order of quadrature rules is needed.

Moreover, in order to take advantage of higher accuracy of the higher order basis function, curved triangles, instead of flat triangles, are needed as demonstrated by Test 1.

Finally, it is important to combine a fast solver, such as Krylov subspace iterative solver with fast multipole methods, with high-order methods as the size of the matrix increases.

APPENDIX A: HIGH-ORDER BASIS FUNCTIONS

A.1. Triangular and triangular patches matching

The high-order basis function for a triangular and triangular patch in Figure 2 can be written as [8]

$$\mathbf{f}(\mathbf{x})=\begin{cases}\dfrac{l}{\sqrt{g^+}}(P_1^+(u_1,u_2)\partial_1\mathbf{x}+P_2^+(u_1,u_2)\partial_2\mathbf{x}) & \text{if } \mathbf{x}=\mathbf{x}^+(u_1,u_2)\in T^+\\ \dfrac{l}{\sqrt{g^-}}(P_1^-(u_1,u_2)\partial_1\mathbf{x}+P_2^-(u_1,u_2)\partial_2\mathbf{x}) & \text{if } \mathbf{x}=\mathbf{x}^-(u_1,u_2)\in T^-\end{cases}$$

where

$$\begin{aligned}P_1^+(u_1,u_2)&=I_n^a g_A(u_1,u_2)+\sum_{m=2}^{M}\frac{I_n^{(m)}-\tilde{I}_t^{(m)}}{2}g_m^{e_2^+}(u_1,u_2)+\sum_{(l,m)\in L_\Delta}c_{lm}^1 g_{lm}^{\text{int}}\\ P_2^+(u_1,u_2)&=I_n^c g_C(u_1,u_2)+\sum_{m=2}^{M}\frac{I_n^{(m)}+\tilde{I}_t^{(m)}}{2}g_m^{e_2^+}(u_1,u_2)+\sum_{(l,m)\in L_\Delta}c_{lm}^2 g_{lm}^{\text{int}}\end{aligned}\tag{A1}$$

and

$$\begin{aligned}P_1^-(u_1,u_2)&=-I_n^a g_A(u_1,u_2)+\sum_{m=2}^{M}\frac{-I_n^{(m)}-\hat{I}_t^{(m)}}{2}g_m^{e_2^-}(u_1,u_2)+\sum_{(l,m)\in L_\Delta}d_{lm}^1 g_{lm}^{\text{int}}\\ P_2^-(u_1,u_2)&=-I_n^c g_C(u_1,u_2)+\sum_{m=2}^{M}\frac{-I_n^{(m)}+\hat{I}_t^{(m)}}{2}g_m^{e_2^-}(u_1,u_2)+\sum_{(l,m)\in L_\Delta}d_{lm}^2 g_{lm}^{\text{int}}\end{aligned}\tag{A2}$$

with $e_2^-=e_2^+=ca$ and

$$L_\Delta=\{(l,m),\ 0\leqslant l+m\leqslant M-3\}\tag{A3}$$

Unknowns for each edge AC are

$$I_n^a, I_n^c, I_n^{(m)}, \tilde{I}_t^{(m)}, \hat{I}_t^{(m)}, \quad 2\leqslant m\leqslant M\tag{A4}$$

and interior unknowns for each triangular patch are

$$c_{lm}^1, c_{lm}^2, d_{lm}^1, d_{lm}^2 \quad (l,m)\in L_\Delta\tag{A5}$$

REFERENCES

1. Harrington RF. *Time Harmonic Electromagnetic Fields*. McGraw-Hill: New York, 1961.
2. Yee KS. Numerical solution of initial boundary value problems involving Maxwell equations in isotropic media. *IEEE Transactions on Antennas and Propagation* 1966; **14**:302–307.
3. Mosig JR. Integral equation technique. In *Numerical Techniques for Microwave and Millimeter—Wave Passive Structure*, Itoh T (ed.). Wiley: New York, 1989; 133–213.
4. Harrington RF. *Field Computation by Moment Methods*. Macmillan: New York, 1968.
5. Sommerfeld A. *Partial Differential Equations in Physics*. Academic Press: New York, 1964.
6. Rao SM, Wilton DR, Glisson AW. Electromagnetic scattering by surfaces of arbitrary shape. *IEEE Transactions on Antennas and Propagation* 1982; **AP-30**:409–418.
7. Cai W, Yu T, Wang H, Yu Y. High order mixed RWG basis functions for electromagnetic applications. *IEEE Transactions on Microwave Theory and Techniques* 2001; **49**:7.
8. Cai W. High order current basis functions for electromagnetic scattering of curved surfaces. *Journal of Scientific Computing* 1999; **14**(1):73–105.
9. Wandzura S. Electric current basis functions for curved surfaces. *Electromagnetics* 1992; **12**:77–91.
10. Popovic BD, Kolundzija BM. *Analysis of Metallic Antennas and Scatters*. IEE Press: UK, 1994.
11. Andersen LS, Volakis JL. Development and application of a novel class of hierarchical tangential vector finite elements for electromagnetics. *IEEE Transactions on Antennas and Propagation* 1999; **47**:(1):112–120.
12. Nedelec JC. Mixed finite elements in R^3. *Numerische Mathematik* 1980; **35**:315–341.
13. Webb JP. Edge elements and what they can do for you. *IEEE Transactions on Magnetism* 1993; **29**: 1460–1465:276–281.
14. Demkowicz L, Vardapetyan L, Rachowicz W. Hp-adaptive edge finite elements for Maxwell equations. *ACES' 98*, Monterey, CA, March 16–20, 1998.
15. Song JM, Chew WC. Moment method solutions using parametric geometry. *Journal of Electromagnetic Waves and Applications* 1995; **9**(1/2):71–83.
16. Sancer MI, McClary RL, Glover KJ. Electromagnetic computation using parametric geometry. *Electromagnetics* 1990; **10**(1–2):85–103.
17. Wilkes DL, Cha C-C. Method of moments solution with parametric curved triangular patches. *1991 International IEEE AP-S Symposium Digest*, London, Ontario, 1991; 1512–1515.
18. Raviart PA, Thomas JM. A mixed finite element method for 2nd order elliptic problems. Lecture Notes in Mathematics, Vol. 606, Springer: Berlin, New York, 1977; 292–315.
19. Nedelec JC. Computation of eddy current on a surface in R^3 by finite element methods. *SIAM Journal of Numerical Analysis* 1978; **15**(3):580–594.
20. Szabo B, Babuska I. *Finite Element Analysis*. Wiley: New York, 1991.
21. Wilton DR, Rao SM, Glisson AW, Schaubert DH, Al-Bundak OM, Butler CM. Potential integrals for uniform and linear source distributions on polygonal and polyhedral domains. *IEEE Transactions on Antennas and Propagation* 1984; **AP-32**(3).
22. Duffy MG. Quadrature over a pyramid or cube of integrands with a singularity at a vertex. *SIAM Journal of Numerical Analysis* 1982; **19**:1260–1262.
23. Kieser R. The triangle-to-square transformation for finite-part integrals. In *Numerical Techniques for Boundary Element Methods.* Proceedings, Kiel, Jan., 1991, Hackbusch W (ed.). Notes on Numerical Fluid Mechanics, Vol. 33. Vieweg: Braunschweig, 1992.
24. Schwab C, Wendland WL. On the numerical cubatures of singular surface integrals in boundary element methods. *Numerische Mathematik* 1992; **62**:343–369.
25. Muller C. *Foundation of the Mathematical Theory of Electromagnetic Waves*. Springer: Berlin, 1969.
26. Harrington RF. Characteristic modes for antennas and scatters. In *Numerical and Asymptotic Techniques in Electromagnetics*, Mittra R (ed.). Topics in Applied Physics, Vol. 3, Springer: Berlin, 1975.
27. Chew WC. *Waves and Fields in Inhomogeneous Media* (2nd edn). IEEE Press: New York, 1995.
28. Senior TB, Volakis JL. *Approximate Boundary Conditions in Electromagnetics*. The Institute of Electrical Engineers: Bath, England, 1994.
29. Kreyszig E. *Differential Geometry*. Dover Publication: New York, 1991.
30. Dunavant DA. High degree efficient symmetrical Gaussian quadrature rules for the triangle. *International Journal for Numerical Methods in Engineering* 1985; **21**:1129–1148.

